Intensity-Modulated Fiber-Optic Sensor: A Novel Grid Measurement Unit

Wenxuan Yao, *Senior Member, IEEE*, Lingwei Zhan, *Member, IEEE*, Sterling Sean Rooke, Christopher Vizas, Victor Kaybulkin, Thomas J. King, Bailu Xiao, *Member, IEEE*, Zhi Li, *Member, IEEE*, Yilu Liu, *Fellow, IEEE*, and He Yin, *Senior Member, IEEE*

***Abstract*—This article presents a novel approach to physical-displacement-based power grid measuring via an intensity-modulated fiber-optic sensor (IMFOS). An IMFOS utilizes one fiber to transmit the intensity modulated light from its electro-optic controller to a fiber-optic probe. The power grid voltage and current can induce physical displacements in transducers via the piezoelectric effect and the Lorentz law, respectively, which then result in a distance change between the optical probe and the reflective surface of the transducers. In parallel, multiple fibers are used to collect the reflective light for electro-optic conversion. A National-Instruments-based characterization platform is set up for performance evaluation. The testing result demonstrates that the IMFOS is immune to the inherent dc and low-frequency saturation issues prevalent in conventional potential and current transformers. Finally, the IMFOS is implemented in a universal grid analyzer to illustrate its applicability for phasor estimation in actual power grids.**

***Index Terms*—Intensity-modulated fiber optic (IMFO), power grid measuring, universal grid analyzer (UGA).**

I. Introduction

HIGH-FIDELITY monitoring devices, such as phasor measurement units (PMUs), play an essential role in improving the reliability and resilience of the power grid by providing real-time measurements of voltage and current [1]–[6]. As the feedback from power system actuators, precise and real-time measurements are the solid foundations and strong supports for power system automation applications, such as distributed energy source controls [7], damping controls [8], power system situational awareness [9], and event localization [10]. For instance, by using the synchrophasors provided by multiple PMUs, a damping controller can mitigate major categories of frequency oscillations and allow more renewable electricity in power grids.

Conventional electromagnetic potential transformers (PTs) and current transformers (CTs) are widely installed to provide a measurement interface for grid monitoring devices. By using both CT and PT, PMUs and the supervisory control and data acquisition systems can provide real-time measurements to the grid control center. Unfortunately, such magnetic-core-based PT/CTs have inherent weaknesses, such as magnetic saturation, electromagnetic interference (EMI) sensitivity, and poor linearity, which typically become one of the bottlenecks for reliable and accurate grid measurements [11]–[13]. For example, the dc component under the fault conditions can cause the saturation of transducers, which would have an adverse impact on the protection functions of the relay and consequently on the system stability [14]. Moreover, the conventional PT and CT require a direct physical connection to a conductor for sensing and, thus, are usually equipped with oil or sulfur hexafluoride gas for insulation. Such specific requirements complicate their installation process and increase overall maintenance costs, especially under conditions of harsh and explosive environments [15], [16]. The electric- and magnetic-field-based noncontact sensor was developed and tested for the synchronized measurement of a high-voltage transmission line, which would dramatically reduce manufacturing and installation costs [17], [18]. However, these wireless sensors lack robustness and can produce large harmonic distortions.

Applications of fiber-optic sensors can be a powerful tool for the measurement of various physical parameters [19], [20]. Since fiber-optics use light rather than electricity, the fiber-optic sensor is not sensitive to EMI and, thus, is superior in such applications with minimal need for dielectrics. Moreover, the optical sensors are able to address the saturation concerns inherent in existing electromagnetic CT and PT. For the application of power grid sensing, the most common approach of existing optical sensors has relied on the interaction between light and an electromagnetic field based on the Faraday and Pockels effects, which rotates an optical probe field polarization state in proportion to the magnetoelectric fields and measures the

Manuscript received 24 January 2022; revised 4 July 2022; accepted 22 July 2022. Date of publication 28 July 2022; date of current version 22 March 2023. This work was supported by the U.S. Department of Energy under the Grid Modernization Grid Modernization Laboratory Consortium program. Paper no. TII-22-0371. *(Corresponding author: He Yin.)*

Wenxuan Yao, Lingwei Zhan, Thomas J. King, Bailu Xiao, and Zhi Li are with the Oak Ridge National Laboratory, Oak Ridge, TN 37831 USA (e-mail: ywxhnu@gmail.com; zhanl@ornl.gov; kingtjjr@ornl.gov; xiaob@ornl.gov; liz2@ornl.gov).

Sterling Sean Rooke and He Yin are with the Department of Electrical Engineering and Computer Science, University of Tennessee, Knoxville, Knoxville, TN 37996 USA (e-mail: srooke@utk.edu; hyin8@utk.edu).

Christopher Vizas and Victor Kaybulkin are with the SmartSenseCom, Vienna, VA 22180 USA (e-mail: cvizas@smartsensecom.com; vkaybulkin@smartsensecom.com).

Yilu Liu is with the Department of Electrical Engineering and Computer Science, University of Tennessee, Knoxville, Knoxville, TN 37996 USA, and also with the Oak Ridge National Laboratory, Oak Ridge, TN 37831 USA (e-mail: liu@utk.edu).

Color versions of one or more figures in this article are available at https://doi.org/10.1109/TII.2022.3194631.

Digital Object Identifier 10.1109/TII.2022.3194631

changes in light phase and polarity, in turn indicating various electric and magnetic phenomena [17]–[26]. However, the effects of light polarization, temperature, filtration calibration, and birefringence drift all adversely impact the performance of these sensors. Moreover, the specialized polarization required by components, coupled with the calibration process, makes the sensor design costly to manufacture.

Compared with the light polarization modulation method, the intensity-modulated fiber-optic (IMFO) approach has merits in its simplicity and robustness [27], [28]. Unlike the light polarization modulation technology, the IMFO does not require interferometry or lasers and is less susceptible to the effects of temperature and vibration. Since IMFO is a promising technology for physical parameter measurement, this article investigates the feasibility of exploiting this technology for power grid voltage and current measurement, with the expectation to overcome the inherent weaknesses in conventional transducers. The proposed intensity-modulated fiber-optic sensor (IMFOS) transmits 850-nm infrared light to its probes via a center fiber. Since the power grid voltage and current can induce physical displacements in transducers via the piezoelectric effect and Lorentz law, respectively, a distance change between the optical probe and the reflective surface of the transducers will occur. Meanwhile, six fibers around the center fiber are used to collect the reflective light, with strength dependent directly on the displacement caused by the physical phenomena of interest. With this in mind, a prototype of IMFOS was fabricated for 120-V/60-Hz power grid monitoring. To evaluate the performance of the prototype sensor, a characterization platform based on the National Instruments (NI) PXI system is built to conduct laboratory experiments, including steady-state dc offset, low frequency, and dynamic tests. Finally, the IMFOS is integrated with a GPS-time synchronized distribution level platform, universal grid analyzer (UGA), to demonstrate its applicability for phasor measurement. The frequency error (FE) and total vector error (TVE) are explored in an actual distribution level power grid. The contributions are summarized as follows.

1) A novel physical-displacement-based power grid measuring technology via an IMFOS is presented, including both real-time voltage and current sensing. Both the working principle and the porotype development of the IMFOS are presented.
2) An NI-based characterization platform is set up for performance evaluation.
3) To thoroughly compare with existing CTs and PTs, multiple experiments are conducted to verify and evaluate the performance of the IMFOS. The IMFOS is also implemented with a PMU in real-world power systems.

The rest of this article is organized as follows. Section II provides the principle of voltage and current probe design based on IMFO technology. Section III presents the mechanism of multireceiving fibers for sensitivity enhancement. Section IV details the IMFOS prototype for distribution power grid sensing. Section V presents the characterization test and UGA implementation to demonstrate the effectiveness of the proposed IMFOS. Finally, Section VI concludes this article.

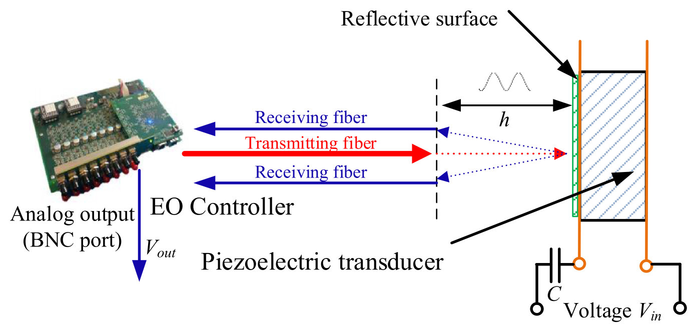

Fig. 1. Structure of the voltage probe in IMFOS.

II. Principal of the Intensity-Modulated Optical Probe

In this section, theoretical foundations for the power grid voltage and current sensing via IMFO technology are discussed. The designs of voltage and current probes are given.

A. Voltage Sensing

According to the piezoelectric effect, a physical displacement will be induced proportional to the potential difference between the two faces of the piezoelectric material [30]. Fig. 1 shows the structure of the voltage probe. The power grid voltage V_{in} is divided via the series capacitor C and the piezoelectric transducer. The relationship between the applied voltage V_{in} and the corresponding displacement Δh of the piezoelectric transducer in height can be expressed as follows:

$$\Delta h = crV_{\text{in}} \tag{1}$$

where c is the constant piezoelectric coefficient of the piezoelectric transducer and r is the reactance ratio between C and the piezoelectric transducer. According to (1), in response to the applied voltage, the piezoelectric transducer will experience a physical displacement, consequently changing the distance between the fiber probe and the reflective surface of the piezoelectric material.

Fig. 1 shows the structure of the voltage probe. To measure the distance, LED light is launched from the electro-optic (EO) controller into a transmitting fiber and then bounced back by the reflective surface of piezoelectric material into receiving fibers. The light propagates via the receiving fibers and is detected by the light-sensing end. Then, the power of the received optical light is converted into an electric current by using a photodiode. Finally, an EO circuit is utilized to generate the output voltage, V_{out}, after filtering and amplification. Therefore, the power grid voltage V_{in}, which is proportional to the displacement of the piezoelectric material, is sensed and converted into V_{out}. The parameters of the IMFOS are listed in Table I.

B. Current Sensing

To sense the current, the IMFOS uses the fiber optic to measure the beam displacement caused by the Lorentz force [31]. Under the Lorentz law, a force F is applied to a charged

TABLE I
PARAMETERS OF THE IMFOS

Parameter	Value/descriptions
V_{in} range	1–120 V
I_{in} range	1–30 A
V_{out} range	0–5 V
Transimpedance gain	5×10^6 V/A
LED emitting wavelength	850 nm
Number of the fiber probe	7
Glass core diameter	200 µm
Plastic cladding	230 µm
Numerical aperture	0.37
Voltage probe material	PZT-4 piezoceramic (Navy Type I)
Voltage probe size	12×1.5×0.5 mm^3
Maximum distance range	500 µm
Sampling rate	50 kHz to 2 MHz

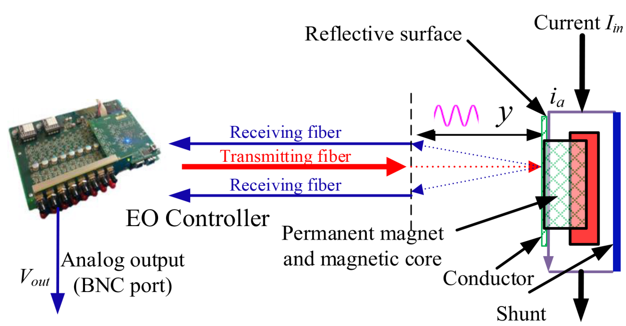

Fig. 2. Structure of the current probe in IMFOS.

particle in a perpendicular direction to both the magnetic field and the current, which can be expressed as follows:

$$F = il \times B \tag{2}$$

where B is the flux dentistry, i is the current in the conductor, and l is the length of the conductor.

As shown in Fig. 2, the power grid current I_{in} is split into the shunt and the conductor a, which is placed in a gap in the magnetic core. A force applied to the conductor a can be expressed as follows:

$$F_a = \frac{\mu i_a}{2\pi d} Bl \tag{3}$$

where $i_a \ll I_{\mathrm{in}}$ and also satisfying $i_a = \mathrm{K}_c I_{\mathrm{in}}$ where K_c is the current divider coefficient depending on shunt parameters. The force F_a creates a displacement Δy of the conductor beam as

$$\Delta y = \frac{5 F_a L^3}{384 EI} \tag{4}$$

where $\frac{5}{384}$ is a constant that depends on how the beam is mounted. E is the modulus of elasticity of the material from which the beam is fabricated, and I is the moment of inertia of the cross section of the beam. L is the length of the beam. Substituting (3) into (4), we can get the following:

$$\Delta y = \frac{5\mu I_{\mathrm{in}} B l L^3 \mathrm{K}_c}{384 EI\pi d}. \tag{5}$$

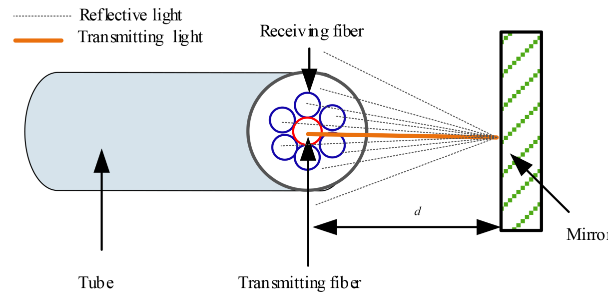

Fig. 3. Probe of optical IMFOS.

It can be seen in (5) that the beam will experience a displacement Δy, which is proportional to I_{in}, toward the direction of the optical probe. Meanwhile, light is launched from the light source into the transmitting fiber and then reflected by the reflective surface of the conductor into the receiving fibers. The light will propagate via the receiving fibers and be detected by the light-sensing end. Therefore, the power grid current I_{in} will be sensed in IMFOS. Then, a similar procedure as discussed in the voltage sensor will be used to convert the receiving optical power into output voltage, V_{out}. The parameters of the current sensor are listed in Table I.

III. MULTIRECEIVING FIBERS

To increase the sensitivity of IMFOS, the multifiber structure is utilized, comprising multiple multimode receiving fibers and one transmitting fiber. The arrangement of the fibers is illustrated in Fig. 3. The transmitting fiber is placed in the center of the bundle and is then symmetrically surrounded by multiple receiving fibers. All of the fibers are held in a tube, such that the ends of each fiber are adjacent by a distance d to the mirror onto transducers exhibiting physical displacement. Because the light is bounced back in all directions on the reflective surface, as shown in Fig. 3, the multiple receiving fiber design is beneficial to capture more reflective light and improve the sensitivity.

In the sensitivity test, the fiber is mounted on a micrometer translator, which can be displaced manually against a mirror mounted on the piezoelectric transducer. The PZT-4 cylinder of 2-inch outer diameter and 3-inch length is utilized, which can vibrate in response to the applied voltage. In the test, the probe is manually displaced by a step of 25.4 μm using the translator. Figs. 4 and 5 illustrate the comparison between multifibers and single fibers with respect to dc and ac displacement sensitivity over d, respectively. For dc displacement sensitivity, it represents the relationship between reflected light power with the probe-mirror distance. For ac displacement sensitivity, it represents the relationship between signal voltage level and probe-mirror distance. With a higher dc and ac sensitivity, a stronger reflected light and a higher voltage of the received signal can be obtained, which indicates an enhanced ability to detect the displacement.

According to the results shown in Fig. 4, the maximum dc sensitivity for one fiber probe occurs at the smallest probe-mirror distance, whereas the maximum sensitivity is achieved at a

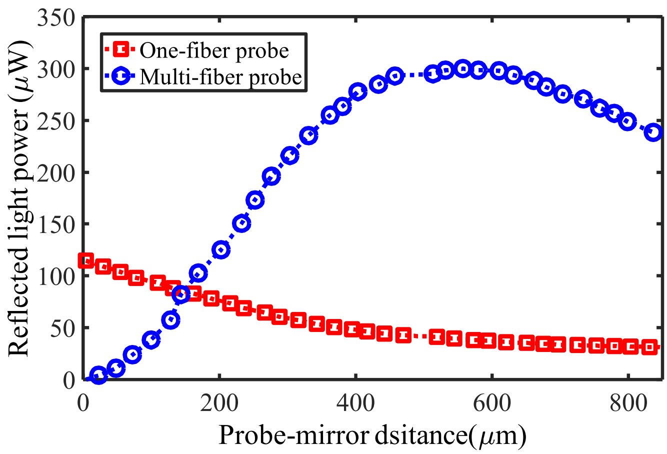

Fig. 4. Comparison of dc displacement sensitivity between multifiber and one-fiber probes.

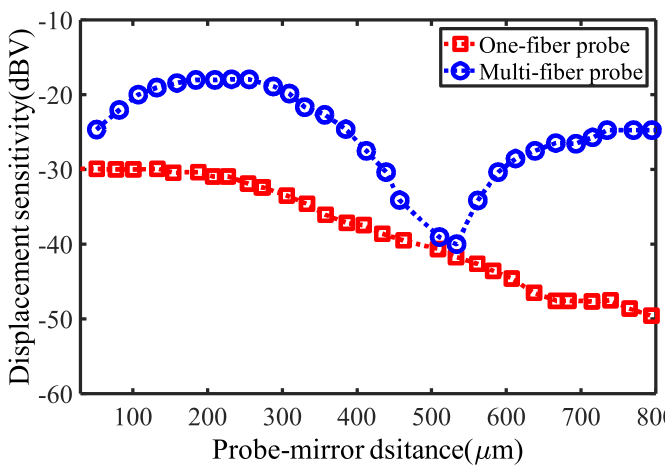

Fig. 5. Comparison of ac displacement sensitivity between multifiber and one-fiber probes.

greater distance for the multifiber probe. Moreover, a significantly higher light power is detected in the multifiber probe. From Fig. 4, the maximum dc displacement sensitivity of the multifiber probe is achieved in the region of 300–600 μm with a significantly higher power of detected light. The largest detected light power of a multifiber probe is 300 μW compared to 110 μW of a single-fiber probe, which indicates the coupler used in the multifiber probe increases the detected light power by about two times larger than that of a single-fiber probe. It can be seen from Fig. 5 that the maximum ac displacement sensitivity of the multifiber probe is approximately 13 dB higher than that of a single-fiber probe. The increased sensitivity makes a multifiber probe a better choice for applications that require high-quality measurements.

IV. Prototype Development

In this section, the prototype of the IMFOS is built for a 120-V/60-Hz distribution power grid. The systematic diagram can be seen in Fig. 6. The maximum and minimum detectable

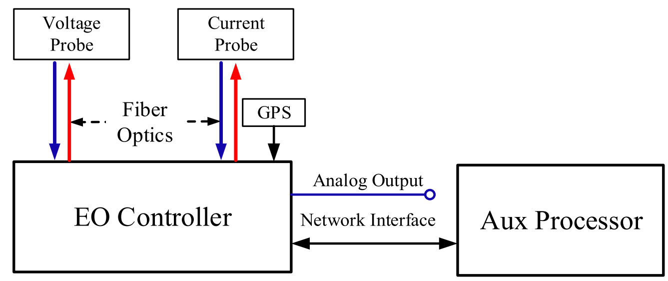

Fig. 6. Diagram of the IMFOS.

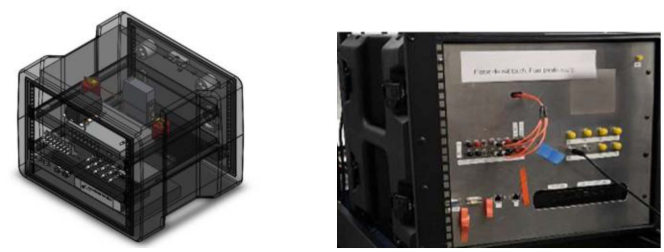

(a) (b)

Fig. 7. Prototype of IMFOS. (a) Structure perspective drawing. (b) Front panel.

voltages are 120 V and 1 V, respectively. The maximum and minimum detectable currents are 30 A and 1 A, respectively. The voltage specification is determined by the selection of series capacitor C and piezoelectric transducer, whereas the current specification is determined by the selection of the conductor. The IMFOS consists of four major components, including a voltage probe, a current probe, an EO controller, and an Aux Processor. A photograph of the prototype is shown in Fig. 7. It is noted that there is no mutual influence between the voltage and the current probes. For the voltage channel, the physical displacement on the piezoelectric transducer is induced in response to the applied voltage via the piezoelectric effect. For the current channel, the physical displacement occurs on the conductor via the Lorentz law. These two displacements are mutually independent of each other and will be captured via two separate optical fiber probes.

The sensor uses an LED emitting at 850-nm wavelengths as a light source with a silicon PIN diode to sense the displacement as discussed in Section III. The fiber probe consists of seven identical multimode fibers with a 200-μm diameter glass core and a 230-μm plastic cladding, with a numerical aperture of 0.37. The transmitting fiber is surrounded by multiple receiving fibers distributed in a fixed geometric pattern. For a voltage probe, a bimorph transducer element constructed from PZT-4 piezoceramic (Navy Type I) with nominal dimensions of 12 $\times$ 1.5 $\times$ 0.5 mm^3 is utilized [32]. It is noted that this kind of piezoelectric material has a cantilever resonance frequency of around 1.5 kHz. Actually, a variety of geometries can be leveraged with dimension selection beforehand to realize a predefined resonance frequency considering the tradeoff between sensitivity and bandwidth. For the current probe, a copper bus bar with a shunt is used as a conductor to pass and divide the current. Voltage drop is taken from the bus bar via its resistive divider for measurement.

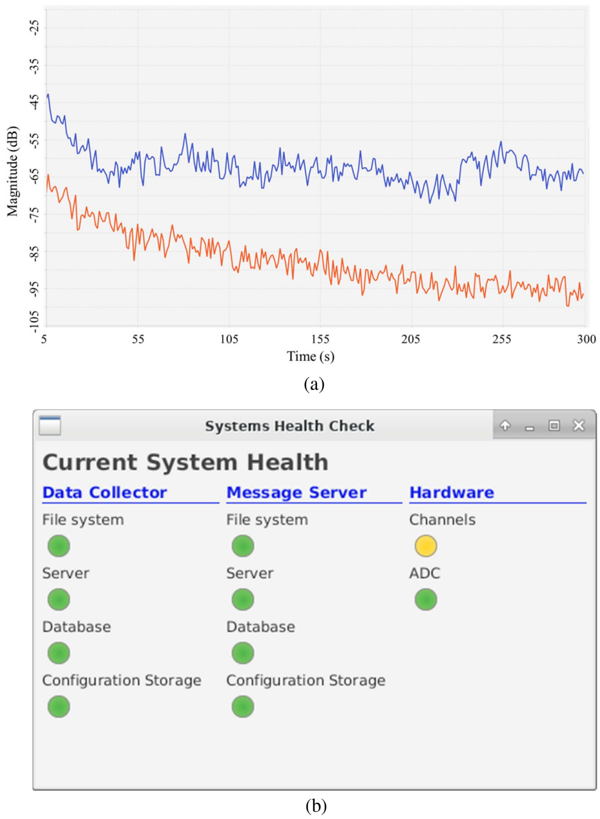

Fig. 8. GUI of the application in the AUX processor. (a) Spectrum of the measured signal. (b) System configuration.

As shown in Fig. 4, the reflected optical power increases with the displacement distance until 500 μm and gradually decreases thereafter. Thus, the quiescent operation point is set at 280 μm with the highest-slope region of the optical response. A photodiode converts the received optical signal into an electric signal in its EO controller. The IMFOS can provide both analog and digital outputs that are converted from the optical signal. The analog output is in the range of 0–5 V. On the other hand, the digital output can be accessed via the network interface. The sampling rate can be adjusted from 50 kHz to 2 mHz. The Aux Processor is a minicomputer with a CentOS7 operating system and an application for digital output visualization as well as the configuration of the IMFOS. Moreover, it will also write the digital output to local files in different data formats, including TDMS, LPCM, and MATLAB. The graphical user interface (GUI) of the application in the Aux Processor can be seen in Fig. 8.

V. Performance Evaluation

In this section, the performance of the IMFOS is evaluated via the sensor characterization platform and UGA. The diagram of the sensor characterization platform is shown in Fig. 9. The platform is built using the NI PXI system, which includes an 18-slot PXIe-1085 chassis, an Intel Core i7 embedded controller PXIe-8135, a 40-MHz arbitrary waveform generator PXIe 5423, and a PXIe 6366 with 8 channels of 16-b analog-to-digital converter (ADC). The predefined reference signal is created in a PXIe-8135 and then sent to a PXIe 5423 for digital-to-analog (DA) conversion. The output analog signal of the PXIe 5423 is then fed into the voltage or current amplifier for sensor characterization. The Trek PZD 700A and AETECHRON 7228 are utilized as the voltage and current amplifiers, respectively. The output waveforms of amplifiers and sensors under test are simultaneously recorded via PXIe 6366 with a 50-kHz sampling rate. As illustrated in Fig. 9, since the PXIe-5423, amplifiers, and IMFOS support bayonet neill–concelman (BNC) ports, the voltage and current signals are sent by BNC cables from the PXIe-5423 to the amplifier and then to the IMFOS. The output signals from IMFOS are converted to general-purpose signal cables and then received by the PXIe-6366.

A. Steady-State Test

In the steady-state test, the steady sinusoidal signal is generated in the NI PXIe 5423 and then fed into the voltage and current amplifiers. The amplitude and frequency responses of the IMFOS are tested, and the results are shown in Fig. 10. For the amplitude response as shown in Fig. 10(a), by analyzing the amplitude response result, the coefficient of determination R^2 of the linear regression can be calculated as follows:

$$R^2 = 1 - \frac{\sum_i (V_i - f_i)^2}{\sum_i (V_i - \bar{V})^2} \tag{6}$$

where V_i and f_i are the voltage-fitted values at index i. $\bar{V}$ is the mean of voltage measurements. In the best case, the voltage values match the fitted values so that R^2 is equal to 1. R^2 of the current measurement can be calculated in a similar method. As illustrated in Fig. 10(a), R^2 is larger than 0.99, which demonstrates the high linearity of the IMFOS. For the frequency response, it is discovered that the IMFOS has a flat region from 10 to 1000 Hz, as illustrated in Fig. 10(b). The overall spectral characteristic of the prototype is impacted by various factors, including piezoelectric/conductor material, low-pass filter in its EO controller, transmitting fiber, and fiber mounting strategy. The effective frequency response range can be defined as the frequencies with amplitudes above the flat region, i.e., 10–3000 Hz. The narrow frequency range is one disadvantage of the proposed sensor. To improve it, one potential solution is to apply an effective filter to filter out the resonant region of the transducer.

B. DC Offset and Low-Frequency Tests

The dc offset and low-frequency tests are conducted by comparing the magnetic CT and PT since the magnetic core transducer is susceptible to dc and low-frequency injection. In this section, the Agilent 6812B and Omicron CMC256 are used to produce voltage and current signals, respectively. First, a 60-Hz sinusoidal waveform superposed with a 20% dc component is generated. From the results presented in Figs. 11 and 12, the saturation effect caused by the dc component can be observed in the output of the magnetic transducer while no negative impact is found for the IMFOS, which demonstrates dc immunity in IMFOS. From Figs. 11(b) and 12(b), the magnetic PT and

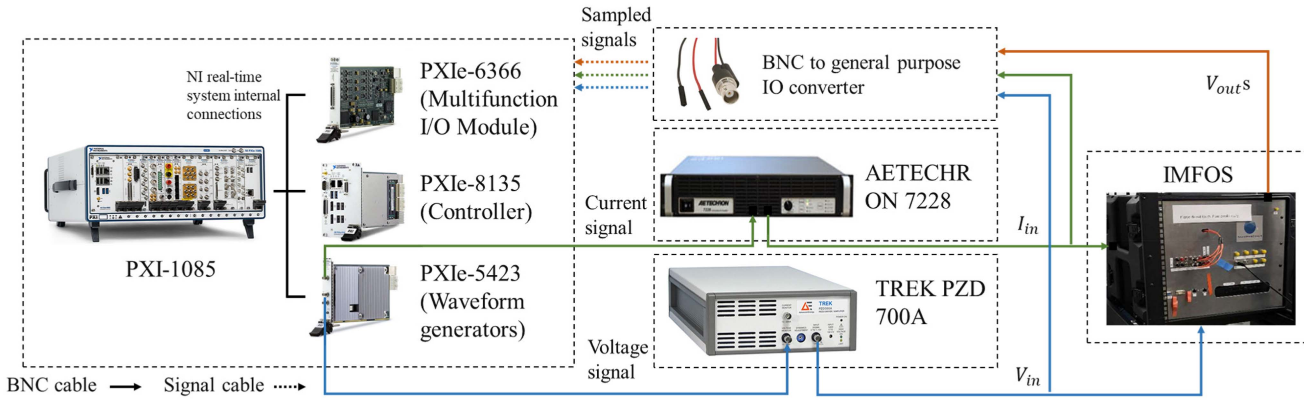

Fig. 9. Diagram of the NI-based sensor characterization platform.

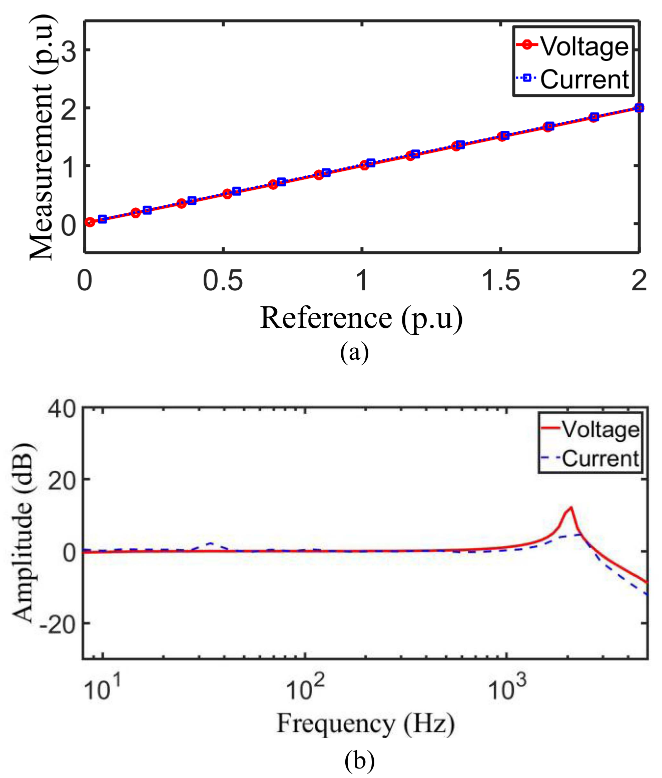

Fig. 10. Result of the steady-state test (a). Amplitude response (b). Frequency response.

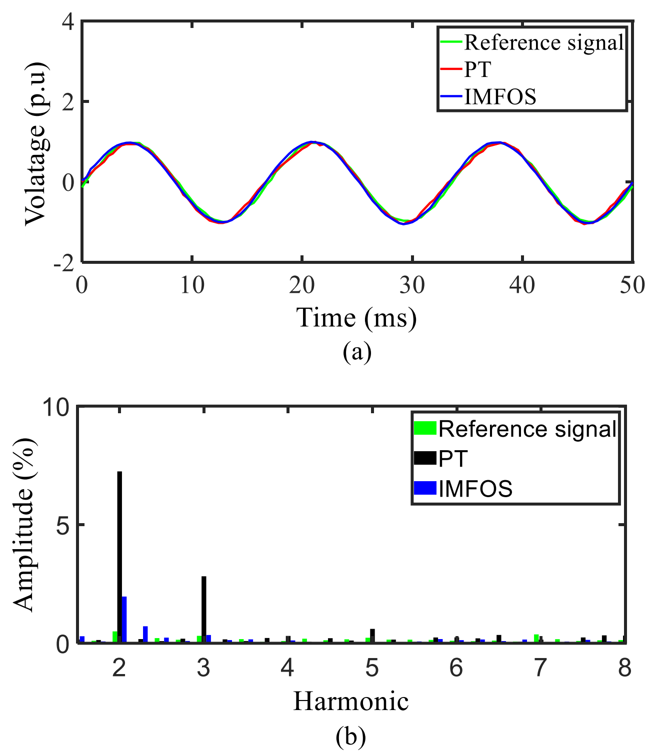

Fig. 11. Voltage test with dc component. (a) Time-domain waveform. (b) Harmonic and interharmonic components.

CT have severe second- and third-harmonic distortions, which make their output unreliable under this circumstance. Thus, the IMFOS outperforms the magnetic-based sensor when the input signal has a dc offset, which could be caused by various factors, such as geomagnetic disturbance, transient grounding fault, or electromagnetic pulse-E3 (EMTP3) [12], [29]. Fig. 13 shows the results of the low-frequency test. A 14.5-Hz sinusoidal frequency component is injected into the sensors under test. Similarly, a severe distortion can be seen for magnetic PT and CT, whereas the saturation effect is successfully eliminated in IMFOS, indicating that the low-frequency signal can be accurately measured by utilizing optic-electric technology. To have a quantitative comparison among the IMFOS, PT, and CT, the voltage and current errors under three test cases are listed in Table II. It can be clearly observed that the voltage errors of the IMFOS are as low as those of the PT under both dc offset and low-frequency tests. However, the current errors of the IMFOS are much lower than those of CTs under two test cases. These results indicate that the voltage measurement accuracy of the IMFOS is as good as PTs, whereas the current measurement accuracy is better than CTs under dc offset and low-frequency test cases.

C. Dynamic Test

The aim of the dynamic test is to assess the capability of the IMFOS for capturing the dynamic behavior of the input signal.

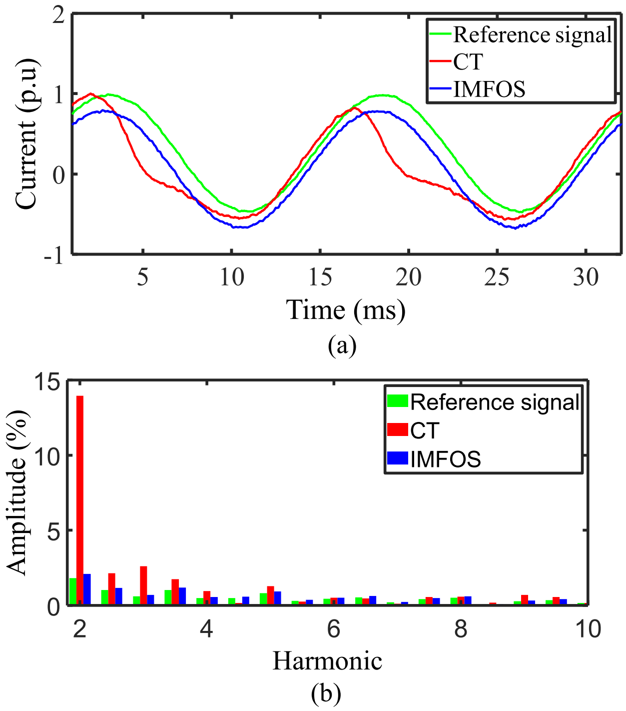

Fig. 12. Current test with dc component. (a) Time-domain waveform. (b) Harmonic and interharmonic.

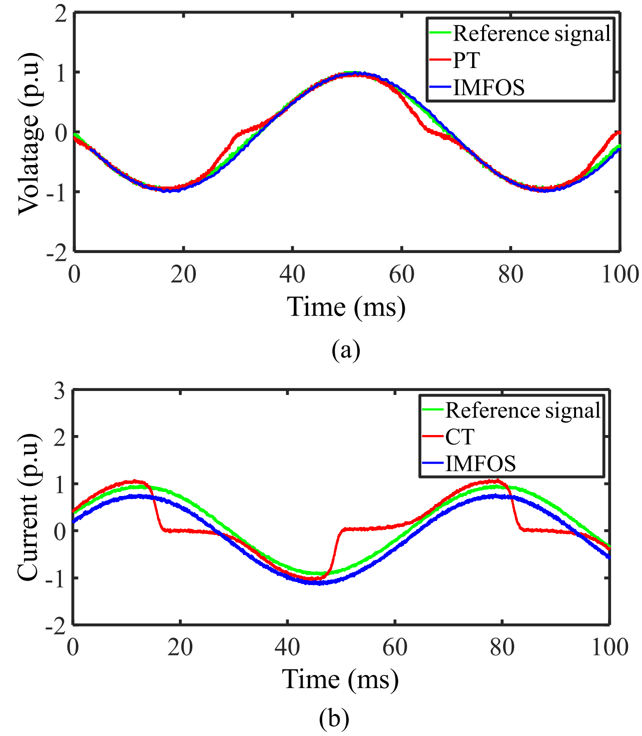

Fig. 13. Test results with low-frequency (14.5 Hz) component. (a) Voltage test. (b) Current test.

TABLE II
COMPARISON AMONG IMFOS, PT, AND CT

Test cases	IMFOS			PT	CT
	Voltage error	Current error	FE	Voltage error	Current error
DC offset test	0.0532 p.u.	0.0036 p.u.	NA	0.0559 p.u.	0.1347 p.u.
Low-frequency test	0.0277 p.u.	0.0065 p.u.	NA	0.0619 p.u.	0.2331 p.u.
Dynamic test	0.00059 p.u.	0.0011 p.u	2 MHz	NA	NA

Step change and ramp for the amplitude and frequency are tested referring to the IEEE C37.118 standard [33]. For the frequency step change test, the frequency of the input signal jumps up from 60 to 61 Hz, stays at 61 Hz for 2 s, and then jumps back down to 60 Hz. For the frequency ramp test, the frequency of the input signal first ramps up from 59.5 to 60.5 Hz in 2 s at a rate of 0.5 Hz/s, stays at 60.5 Hz for 2 s, then ramps down from 60.5 to 59.5 Hz in 2 s at a rate of −0.5 Hz/s. The amplitude dynamic tests employ similar change characteristics as the frequency dynamic tests. The testing results are shown in Figs. 14 and 15. The recursive discrete Fourier transform is adopted for the frequency calculation, and the root mean square is calculated to obtain voltage and current amplitude. From the results, the reference signal and output of IMFOS match well, which verifies the ability of the IMFOS to track the dynamic behavior of signals. Again, a quantitative analysis of the IMFOS is listed in Table II under the dynamic test. The results show that both the voltage and current measurements are very precise under dynamic tests.

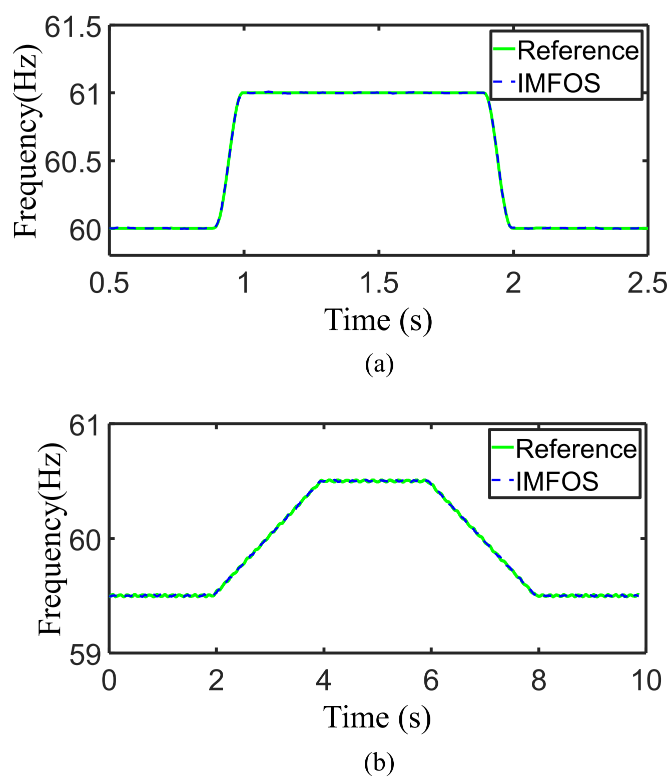

Fig. 14. Frequency dynamic test. (a) Voltage frequency step change. (b) Current frequency ramp.

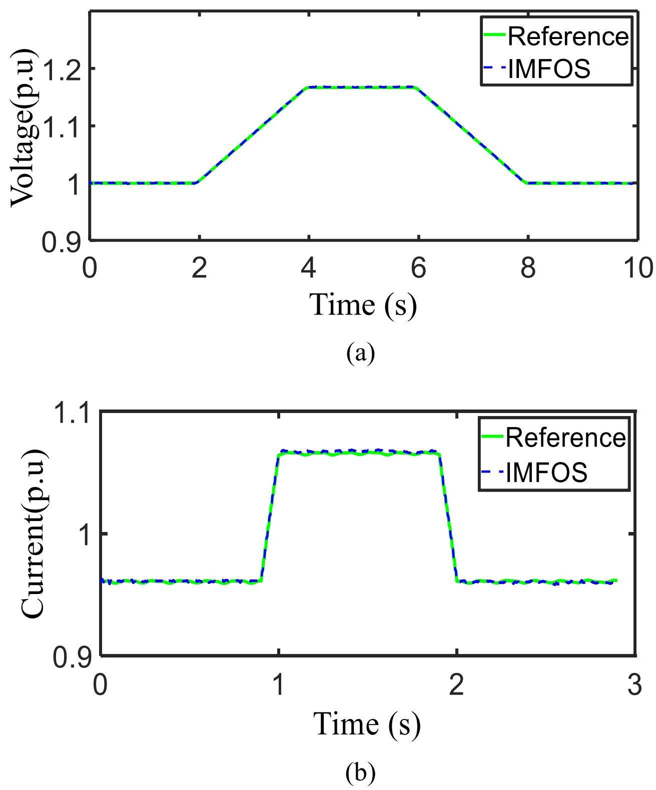

Fig. 15. Amplitude dynamic test. (a) Voltage amplitude ramp. (b) Current amplitude step change.

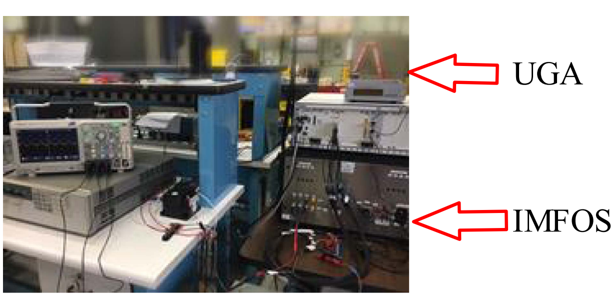

Fig. 16. Test setup for UGA implementation.

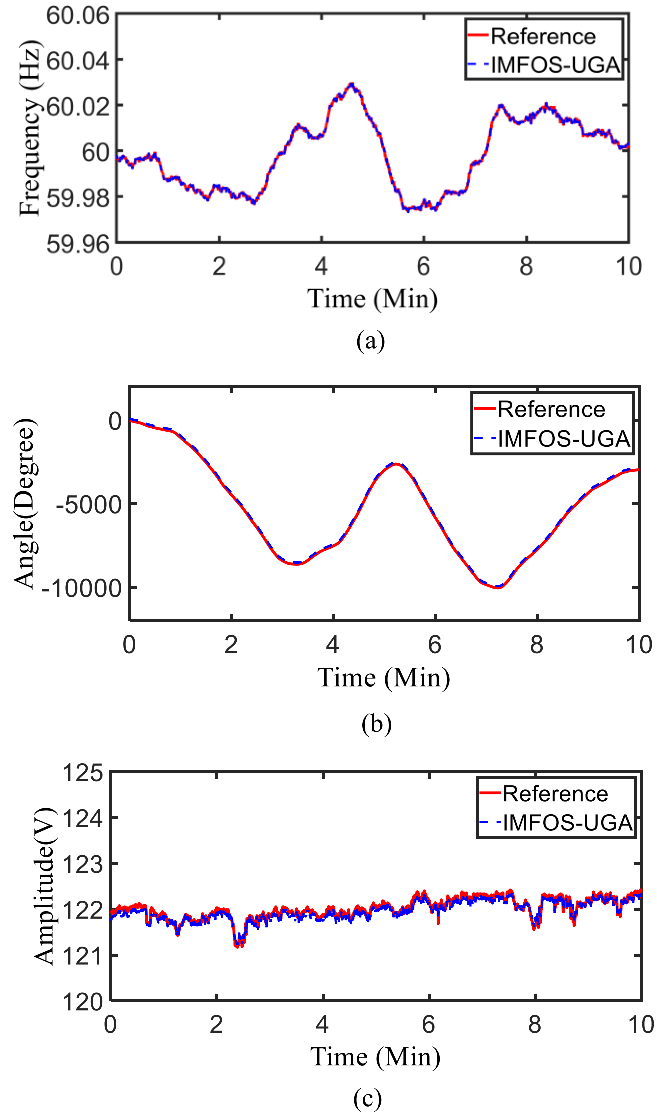

Fig. 17. Test result for IMFOS-UGA. (a) Frequency. (b) Angle. (c) Amplitude.

In addition, the average FE is 2 mHz, which is lower than the PMU frequency measurement requirement under a frequency ramp test listed in the IEEE C37.118.1 [33].

D. Implementation in UGA

To demonstrate the applicability of IMFOS for phasor estimation in an actual power grid, the IMFOS is implemented in the UGA platform, referred to as IMFOS-UGA, as shown in Fig. 16. The IMFOS is connected to a distribution power grid and provides input signals to a UGA for synchronized frequency, angle, and magnitude measurements. For the sake of comparison, a normal UGA with accuracies of 1m Hz for the frequency, 0.05 V for the voltage magnitude, and 0.05° for the angle is set up as a reference. The two UGAs are time synchronized by GPS signal throughout the test; thus, the measurements can be aligned with the coordinated universal time (UTC) timestamp. The results of the frequency, angle, and voltage magnitude measurements are shown in Fig. 17(a)–(c). It can be seen in Fig. 17 that the IMFOS-UGA has the capability to synchronously capture the trends of its frequency, angle, and amplitude over time. The FE and TVE are as small as 2 mHz and 0.029%, which are sufficient to comply with the 5m Hz and 1% requirement of the IEEE PMU standard C37.118.1 [33]. It is worth mentioning that UGA is utilized as an example platform for synchronized power grid monitoring. Since the output analog signal of the sensor is 0–5 V dc, it is easily integrated with any other kinds of existing power grid measurement devices, such as PMUs and power quality analyzers, for repeatable tests.

VI. Conclusion

In this article, the IMFOS was developed to monitor grid voltage and current via the measurement of the physical displacement of transducers caused by the piezoelectric effect and the Lorentz force with the advantage of simplicity. The IMFO light was transmitted to the transducers via a one-center fiber and reflected by the mirrors in the transducers. Then, multiple multimode fibers symmetrically surrounding the center fiber with enhanced sensitivity were exploited to collect the reflected signal to its EO controller. A prototype was built to demonstrate the feasibility; its performance was evaluated via an NI-based characterization platform under conditions of both steady and dynamic states, dc, and low-frequency interferences. Experimental results demonstrated its linearity and ability to capture dynamic changes in measured voltage and current signals. This also verified its merit for dc and low-frequency immunity compared to the conventional magnetic PT and CT, indicating that the IMFOS would be a promising tool for electric grid monitoring. Finally, the prototype of IMFOS was implemented on the UGA platform to demonstrate its applicability for distribution power grid phasor monitoring. The FE and TVE of the IMFOS-UGA met the 5 mHz and 1% requirements outlined in the IEEE PMU C37.118 standard.

It is noted that the major elements of the IMFOS, including LED, fiber, conductor, piezoelectric material, and copper busbar, are commonplace. With high-volume production in mind, the cost of the IMFOS will no doubt be competitive with conventional PT and CT. Future research will focus on noise reduction and robustness improvement. Penitential solutions include 1) integration of an effective filter to filter out the resonant region and low-frequency noise, and 2) temperature compensation for the whole EO system.

References

[1] Z. Li, H. Liu, J. Zhao, T. Bi, and Q. Yang, "A power system disturbance classification method robust to PMU data quality issues," *IEEE Trans Ind. Inform.,* vol. 18, no. 1, pp. 130–142, Jan. 2022, doi: 10.1109/TII.2021.3072397.

[2] J. Zhang, H. Wen, and L. Tang, "Improved smoothing frequency shifting and filtering algorithm for harmonic analysis with systematic error compensation," *IEEE Trans Ind. Electron.*, vol. 66, no. 12, pp. 9500–9509, Dec. 2019.

[3] Y. Cui, F. Bai, R. Yan, T. Saha, R. K. L. Ko, and Y. Liu, "Source authentication of distribution synchrophasors for cybersecurity of microgrids," *IEEE Trans. Smart Grid*, vol. 12, no. 5, pp. 4577–4580, Sep. 2021, doi: 10.1109/TSG.2021.3089041.

[4] W. Wang et al., "Frequency disturbance event detection based on synchrophasors and deep learning," *IEEE Trans. Smart Grid.*, vol. 11, no. 4, pp. 3593–3605, Jul. 2020, doi: 10.1109/TSG.2020.2971909.

[5] Y. Cui et al., "Multifractal characterization of distribution synchrophasors for cybersecurity defense of smart grids," *IEEE Trans. Smart Grid*, vol. 13, no. 2, pp. 1658–1661, Mar. 2022, doi: 10.1109/TSG.2021.3132536.

[6] S. Liu et al., "Data-driven event detection of power systems based on unequal-interval reduction of PMU data and local outlier factor," *IEEE Trans. Smart Grid*, vol. 11, no. 2, pp. 1630–1643, Mar. 2020.

[7] A. Alsabbagh, B. Wu, and C. Ma, "Distributed electric vehicles charging management considering time anxiety and customer behaviors," *IEEE Trans Ind. Inform.*, vol. 17, no. 4, pp. 2422–2431, Apr. 2021, doi: 10.1109/TII.2020.3003669.

[8] K. Sun et al., "WAMS-based HVDC damping control for cyber attack defense," *IEEE Trans. Power Syst.*, early access, Apr. 19, 2021, doi: 10.1109/TPWRS.2022.3168078.

[9] L Zhu et al., "Adding power of artificial intelligence to situational awareness of large interconnections dominated by inverter-based resources," *High Voltage*, vol. 6, no. 6, pp. 924–937, Dec. 2021.

[10] S Liu et al., "Data-driven event detection of power systems based on unequal-interval reduction of PMU data and local outlier factor," *IEEE Trans. Smart Grid.*, vol. 11, no. 2, pp. 1630–1643, Mar. 2020.

[11] A. G. Phadke and J. S. Thorp, "Synchronized phasor measurements and their applications," in *Power Electronics and Power Systems*. New York, NY, USA: Springer, 2017.

[12] *IEEE Guide for the Application of Current Transformers Used for Protective Relaying Purposes*, IEEE Standard C37.110-2007 (Revision of Standard C37.110-1996), 2008, pp. 1–90.

[13] G. Franceschini, E. Lorenzani, and G. Buticchi, "Saturation compensation strategy for grid connected converters based on line frequency transformers," *IEEE Trans. Energy Convers.*, vol. 27, no. 2, pp. 229–237, Jun. 2012.

[14] *IEEE Recommended Practice for the Application of Instrument Transformers in Industrial and Commercial Power Systems*, IEEE Standard 3004.1-2013, May 2013, pp. 1–48.

[15] W. Yao et al., "Utilization of optical sensors for phasor measurement units," *Electric Power Syst. Res.*, vol. 156, pp. 12–14, 2018.

[16] P. Niewczas and J. R. McDonald, "Advanced optical sensors for power and energy systems applications," *IEEE Instrum. Meas. Mag.*, vol. 10, no. 1, pp. 18–28, Feb. 2007.

[17] W. Yao and et al., "Pioneer design of non-contact synchronized measurement devices using electric and magnetic field sensors," *IEEE Trans. Smart Grid*, vol. 9, no. 6, pp. 5622–5630, Nov. 2018.

[18] W. Yao, H. Lu, M. J. Till, W. Gao, and Y. Liu, "Synchronized wireless measurement of high-voltage power system frequency using mobile embedded systems," *IEEE Trans. Ind. Electron.*, vol. 65, no. 3, pp. 2775–2784, Mar. 2018.

[19] E. Udd and W. B. Spillman, Jr, Eds., *Fiber Optic Sensors: An Introduction for Engineers and Scientists*. New York, NY, USA: Wiley, 2011.

[20] K. Bremer et al., "Fibre optic pressure and temperature sensor for geothermal wells," in *Proc. SENSORS*, Kona, HI, USA, 2010, pp. 538–541.

[21] J. Li, H. Liu, T. Bi, and J. Zhao, "Second-order matrix pencil-based phasor measurement algorithm for P-class PMUs," *IET Gener., Transmiss. Distrib.*, vol. 14, no. 19, pp. 3953–3961, 2020.

[22] H. Wang, C. Zhuang, R. Zeng, S. Xie, and J. He, "Transient voltage measurements for overhead transmission lines and substations by metal-free and contactless integrated electro-optic field sensors," *IEEE Trans. Ind. Electron.*, vol. 66, no. 1, pp. 571–579, Jan. 2019.

[23] Z. Li, H. Liu, J. Zhao, T. Bi, and Q. Yang, "A power system disturbance classification method robust to PMU data quality issues," *IEEE Trans. Ind. Inform.*, vol. 18, no. 1, pp. 130–142, Jan. 2022, doi: 10.1109/TII.2021.3072397.

[24] W. Sima, R. Han, Q. Yang, S. Sun, and T. Liu, "Dual LiNbO3 crystal-based batteryless and contactless optical transient overvoltage sensor for overhead transmission line and substation applications," *IEEE Trans. Ind. Electron.*, vol. 64, no. 9, pp. 7323–7332, Sep. 2017.

[25] S. Xu, H. Liu, and T. Bi, "A novel frequency estimation method based on complex bandpass filters for P-class PMUs with short reporting latency," *IEEE Trans. Power Del.*, vol. 36, no. 6, pp. 3318–3328, Dec. 2021, doi: 10.1109/TPWRD.2020.3038703.

[26] R. Daniel, "Monitoring electrical assets for fault and efficiency correction," U.S. Patent 7 714 735, 2006.

[27] N. Lagakos, V. Kaybulkin, P. Hernandez, and C. Vizas, "Fiber optic electromagnetic phenomena sensors," U.S. Patent 9 823 277, 2017.

[28] T. Lan, C. Zhang, S. Fu, B. Zhu, M. Tang, and W. Tong, "Spatial division multiplexing-based reflective intensity-modulated fiber optics displacement sensor," *IEEE Photon. J.*, vol. 10, no. 4, pp. 1–7, Aug. 2018.

[29] W. Yao and et al., "Magnetic field based wireless GMD/EMP-E3 impact monitoring device," U.S. Patent 20 180 136 267.

[30] Z. Wu, "A wide linearity range current sensor based on piezoelectric effect," *IEEE Sensors J.*, vol. 17, no. 11, pp. 3298–3301, Jun. 2017.

[31] D. Roylance, *Beam Displacements*. Cambridge, MA, USA: Dept. Mater. Sci. Eng., MIT, 2000, pp. 1–12.

[32] U.S. Department of Defense, "Military standard: Piezoelectric ceramic material and measurements guidelines for sonar transducers," 1995.

[33] *IEEE Standard for Synchrophasor Measurements for Power Systems*, IEEE Standard C37.118.1-2011, Dec. 2011.

Wenxuan Yao (Senior Member, IEEE) received the B.S. degree from the College of Electrical and Information Engineering, Hunan University, Changsha, China, in 2011, and the Ph.D. degree from the Department of Electrical Engineering and Computer Science, University of Tennessee, Knoxville, Knoxville, TN, USA, in 2018, both in electrical engineering.

He is currently a Professor with Hunan University. From 2018 to 2020, he was a Research Associate with Oak Ridge National Laboratory. His research interests include wide-area monitoring systems, phasor measurement unit application, embedded system development, power quality, and big data analysis in power systems.

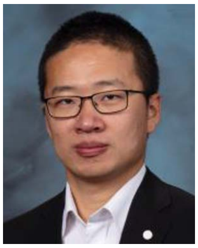

Lingwei Zhan (Member, IEEE) received the B.S. and M.S. degrees in electrical engineering from Tongji University, Shanghai, China, in 2008 and 2011, respectively, and the Ph.D. degree in electrical engineering from the Department of Electrical Engineering and Computer Science, University of Tennessee, Knoxville, Knoxville, TN, USA, in 2015.

He is currently an R&D staff member with Oak Ridge National Laboratory, Oak Ridge, TN, USA. His research interests include advanced grid monitors, phasor measurement units, synchrophasor measurement algorithms, wide-area power system monitoring, renewable energy sources, flexible AC transmission system (FACTs), and HVdc.

Sterling Sean Rooke received the Ph.D. degree in engineering from the University of Maryland College Park, College Park, MD, USA.

He is a Researcher with the Electrical Engineering Department, University of Tennessee, Knoxville, Knoxville, TN, USA. As an Entrepreneur, he leads both X8 LLC, Hanover, MD, USA, and Brixon, Inc., Catonsville, MD, USA, as they advance cyberspace technologies, including machine learning informed industrial controls. As a Reserve Military Officer, he advises the U.S. Government and Air Force in the areas of cyber and technology matters. He was previously an Active Duty Information Warfare Officer in the United States Navy, where he was the Command small business innovation research (SBIR) Lead and assigned to intelligence advanced research projects activity (IARPA). Previously as a civilian, his research interests include optics, wireless, and electromechanical packaging concerns. His early laboratory research work was in the areas of polymer chemistry and biotechnology.

Dr. Rooke was the Communications Division Director for international society of automation (ISA) and an Instrumentation Measurement Chapter Chair for the IEEE.

Christopher Vizas received the undergraduate, graduate and legal education degrees from Yale University, New Haven, CT, USA.

He is currently the Chairman of SmartSenseCom Inc., Vienna, VA, USA.

Victor Kaybulkin received the Ph.D. degree in electrical engineering from the Department of Electronics and Radio Wave Physics, Lobachevsky State University of Nizhny Novgorod - National Research University, Nizhny Novgorod, Russia.

He is currently a Senior Scientist with SmartSenseCom Inc., Vienna, VA, USA. His research interests include fiber-optic sensor research, design, and development.

Thomas J. (Tom) King received the B.S. degree in mechanical engineering from Clarkson University, Potsdam, NY, USA, the M.S. degree in materials engineering from Rensselaer Polytechnic Institute, Troy, NY, in 1993, and the master's degree in business administration from the University of Tennessee, Knoxville, Knoxville, TN, USA.

He has a dual role with the Oak Ridge National Laboratory (ORNL), Oak Ridge, TN, USA, and the University of Tennessee. He is the Director of the Sustainable Electricity Program, ORNL, where he is responsible for leading, coordinating, and implementing ORNL's research and development portfolio of projects conducted for the U.S. Department of Energy (DOE)'s Office of Energy Efficiency and Renewable Energy and Office of Electricity Delivery and Energy Reliability. He is the Director of Industry and Innovation with the University of Tennessee for the jointly funded NSF-DOE Engineering Research Center, Center for Ultra-Wide-Area Resilient Electric Energy Transmission Networks.

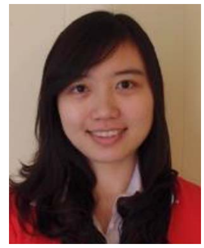

Bailu Xiao (Member, IEEE) received the B.S. and M.S. degrees in electrical engineering from the Huazhong University of Science and Technology, Wuhan, China, in 2006 and 2008, respectively, and the Ph.D. degree in electrical engineering from the University of Tennessee, Knoxville, Knoxville, TN, USA, in 2014.

She is an R&D staff member with Oak Ridge National Laboratory, Oak Ridge, YN, USA. Her current research interests include power electronics system integration, multilevel converters, and microgrid modeling and control.

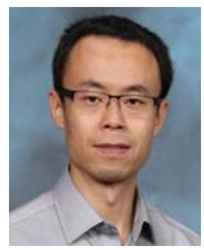

Zhi Li (Member, IEEE) received the B.S.E.E. and M.S. degrees in electrical engineering from Tsinghua University, Beijing, China, in 2000 and 2003, respectively, and the Ph.D. degree in electrical engineering from Washington State University, Pullman, WA, USA.

He is a Research Group Leader with the Sichuan Energy Internet Research Institute, Tsinghua University. He was with the Oak Ridge National Laboratory, U.S. Department of Energy, as a Postdoctoral Research Associate and then an R&D staff member from 2012 to 2022. His research areas include power system analysis, electromagnetic field modeling and analysis for power grid applications, and high-voltage engineering.

Yilu Liu (Fellow, IEEE) received the B.S. degree in 1982 from Xian Jiaotong University, China, and the M.S. and Ph.D. degrees in electrical engineering from Ohio State University, Columbus, OH, USA, in 1986 and 1989, respectively.

She is currently the Governor's Chair with the University of Tennessee, Knoxville (UTK), Knoxville, TN, USA, and Oak Ridge National Laboratory (ORNL), Oak Ridge, TN, USA. She was elected as a member of the National Academy of Engineering in 2016. She is also the Deputy Director of the DOE/NSF-cofunded engineering research center, Center for Ultra-Wide-Area Resilient Electric Energy Transmission Networks. Prior to joining UTK/ORNL, she was a Professor with Virginia Tech, where she led the effort to create the North American power grid frequency monitoring network, which is currently operated at UTK and ORNL as GridEye. Her current research interests include power system wide-area monitoring and control, large interconnection-level dynamic simulations, electromagnetic transient analysis, and power transformer modeling and diagnosis.

He Yin (Senior Member, IEEE) received the B.S. and Ph.D. degrees in electrical and computer engineering from the University of Michigan-Shanghai Jiao Tong University Joint Institute, Shanghai Jiao Tong University, Shanghai, China, in 2012 and 2017, respectively.

He is currently a Research Assistant Professor with the Center for Ultra-Wide-Area Resilient Electric Energy Transmission Networks, University of Tennessee, Knoxville, Knoxville, TN, USA. His research interests include optimization and decentralized control of microgrids, phasor measurement unit design, and power system situational awareness.